# Degradation of Alzheimer's Amyloid-β by a Catalytically Inactive Insulin Degrading Enzyme

Bikash R. Sahoo,[a] Wenguang Liang,[b] Wei-Jen Tang[b] and Ayyalusamy Ramamoorthy*[a]

Email: ramamoor@umich.edu

## Abstract

Insulin-degrading-enzyme (IDE) is a key target to treat type-2 diabetes, and also known to clear Alzheimer's amyloid-β (Aβ). However, the development of catalytically inactive IDE mutant ($_{E111Q}$IDE) could risk Aβ clearance. Here, we demonstrate Aβ degradation by $_{E111Q}$IDE and the removal of zinc from the toxic Aβ-Zn complex enabling proteolysis by IDE. Fluorescence and NMR results show delays in Aβ aggregation by both wild-type and $_{E111Q}$IDE in their zinc-bound and unbound states. Diffusion NMR and LC-MS revealed the delayed kinetics is due to Aβ degradation. Remarkably, IDEs exhibited no proteolysis against zinc bound Aβ species as evidenced from high-speed AFM, electron microscopy, chromatography and NMR. On the other hand, zinc removal from the Zn-Aβ complex enabled the proteolysis by IDEs. These findings highlight the role of zinc in switching on/off the proteolysis of Aβ and urge the development potent zinc chelators as a strategic alternative therapeutic for AD.

Amyloid-β (Aβ) aggregation is a key molecular factor contributing to Alzheimer's disease (AD) by impairing synaptic function via neuronal cell death.[1,2] Two major Aβ isoforms Aβ(1-40) and Aβ(1-42) are targeted in controlling AD progression.[3] The anti-amyloid immunotherapy is a promising strategy to control AD progression that includes the inhibition of Aβ aggregation, reduction of the formation of soluble neurotoxic oligomers, rapid fibrillation, and generation of amorphous aggregates.[4,5] Unfortunately, till date, there is no success in the therapeutic development.[6] The failure in targeting Aβ could be due to several factors that are poorly understood at the molecular level.[6] While Aβ plaque deposition is moderately correlated to AD, plaque deposition as such has been identified in healthy brains without dementia.[7,8] Also, the involvement of other cellular components (such as membrane, metal ions, enzymes, and apolipoproteins) during Aβ aggregation restricts the strategy for a successful therapeutic development.[9–11] For example, the interaction of water-soluble Aβ with membrane or metal ions (like $Zn^{2+}$ and $Cu^{2+}$) generates amorphous or low-molecular weight oligomers that are highly polymorphic and vary in neurotoxicity.[12–16] Recent studies have identified the metal bound Aβ species to be highly stable and toxic and pathologically crucial targets.[17,18] Metal ion binding to amyloid peptides can affect their enzymatic degradation.[19–21] Reduction in Aβ accumulation is evidenced by enzymes such as insulin-degrading enzyme (IDE), neprilysin (NEP), endothelin-converting enzyme, and matrix metalloproteinase-9.[22–27] IDE and NEP are reported to clear soluble Aβ, whereas matrix metalloproteinase-9 enzyme was found to degrade both soluble and Aβ fibers.[28] IDE, a conserved $Zn^{2+}$ metallopeptidase, selectively interacts with Aβ monomers[29], and its activity is mediated by the dynamic equilibrium between soluble Aβ monomers and aggregates.[30] The IDE-bound Aβ40 structure reveals a catalytic chamber of size ~35 Å suitable to degrade short peptides.[31] Importantly, the inhibition of IDE's activity by small molecule inhibitors[32] or by the development of catalytically inactive mutant ($_{E111Q}$IDE)[33] could suppress Aβ degradation associated with AD.[34] Here, we demonstrate Aβ degradation by $_{E111Q}$IDE, an important targeted enzyme to treat type-2 diabetes, and the role of zinc in the dysfunction of IDEs.

The catalytic rates of $_{wt}$IDE and $_{E111Q}$IDE were tested on the rate of hydrolysis of a bradykinin-mimetic fluorogenic peptide, substrate V.[35] Results showed that $_{wt}$IDE is active on substrate V hydrolysis whereas $_{E111Q}$IDE mutant and IDE variants co-incubated with EDTA ($_{wt}$IDE$^{EDTA}$ and $_{E111Q}$IDE$^{EDTA}$) are not (Fig. S1). Enzymatic degradation activities of $_{wt}$IDE and an inactive $_{E111Q}$IDE mutant were tested, in the absence and presence of EDTA, on Aβ40 using thioflavin-T (ThT) fluorescence assay. At sub-nanomolar IDE concentrations (enzyme:Aβ=1:1000 or 1:250), $_{E111Q}$IDE exhibited a small increase in the lag-time of Aβ aggregation as compared to $_{wt}$IDE that showed no ThT fluorescence (Fig. S2). When mixed with EDTA, $_{wt}$IDE showed substantial delay, whereas $_{E111Q}$IDE$^{EDTA}$ showed a small delay, on the aggregation kinetics (Fig. S2). Remarkably, at superstoichiometric nconcentration

[a] Dr. B.R. Sahoo, Prof. A. Ramamoorthy
Biophysics and Department of Chemistry,
University of Michigan, Ann Arbor, MI 48109 (USA)
[b] Dr. W. Liang, Prof. W. Tang
Ben-May Department for Cancer Research, The University of Chicago, Chicago, IL 60637 (USA)
[*] Prof. Ayyalusamy Ramamoorthy
E-mail: ramamoor@umich.edu

Supporting information for this article is given via a link at the end of the document

(enzyme:Aβ=1:10), all IDE variants showed substantial enzymatic degradation activities illustrating no Aβ40 aggregation up to day 12 (Fig. S3).[30,36] Zinc chelated IDE variants pre-incubated with EDTA also showed substantial catalytic activity and no Aβ aggregation (Fig. S3). These results suggest that IDE variants are active against Aβ40 aggregation despite selective mutation or zinc chelation. Although the concentration of IDE is higher than Aβ in brain, the threshold $_{E111Q}$IDE concentration used in this study (0.5 μM) is ten times lower than Aβ40 indicating the efficiency of the enzyme to treat type-2 diabetes and AD.[37] It should be noted that, the ThT fluorescence quenching in the presence of IDE mutant could also be due to a possible chaperonin activity of IDE.[36,38] To address this, we hypothesize that under a catalytic environment, IDE and its variants will generate fragments of Aβ40.[30] In contrast, under a chaperonin environment, there will be an increase in Aβ40 size due to aggregation or no change due to inhibition .[36]

Strikingly, HPLC-mass spectrometry (LC-MS) analysis identified Aβ40 fragments in all three IDE samples ($_{wt}$IDE, $_{E111Q}$IDE and $_{E111Q}$IDE$^{EDTA}$) with molecular weights varying from >200 to <800 Da (Figs. 1 and S4-S6). It should be noted that although IDE cleaved Aβ fragments can be larger or smaller than 1-kDa (see Fig. S7), the large size fragments (typically >1-kDa) have a tendency to aggregate[30] and are removed using a 10-kDa filter prior to LS-MS measurement in this study. The findings from LC-MS were further confirmed using diffusion ordered NMR spectroscopy (DOSY) in real time. DOSY results revealed ~3 hours incubation of 1:10 $_{wt}$IDE:Aβ presented small (diffusion constant "D"= $2.2\times10^{-6}$ cm$^2$/s) and large ($6.5\times10^{-7}$ cm$^2$/s) size species (Figs. 1D and S8). In addition, similar to $_{wt}$IDE, several small Aβ40 fragments were identified in the presence of $_{E111Q}$IDE with the diffusion constant varying between $0.6\times10^{-6}$ and $3\times10^{-6}$ cm$^2$/s (Fig. 1C,D); based on the DOSY experiments on known molecular weight short peptides (Fig. S9), the observed small Aβ40 fragments are expected to be ~300 Da in size. This observation is remarkable as it rules out non-chaperone activity for both IDEs. Thus, these results from LC-MS and NMR confirm the catalytic activities of $_{wt}$IDE, $_{E111Q}$IDE and zinc-chelated $_{E111Q}$IDE$^{EDTA}$ against Aβ40. Unlike Aβ40 that formed fibrils after ~24 hours of incubation (Fig. S10), Aβ incubated with $_{wt}$IDE, $_{E111Q}$IDE and $_{E111Q}$IDE$^{EDTA}$ generated globular species (Fig. 1H-J). The presence of morphologically similar Aβ species in both wild-type and mutant IDE mixture suggests a similar proteolytic activity. This further correlates to the LC-MS and NMR observations. Although, fluorescence, TEM and LC-MS results correlate with each other, none of these provides substantial information about the aggregation of the degraded Aβ40 fragments. To test this, we

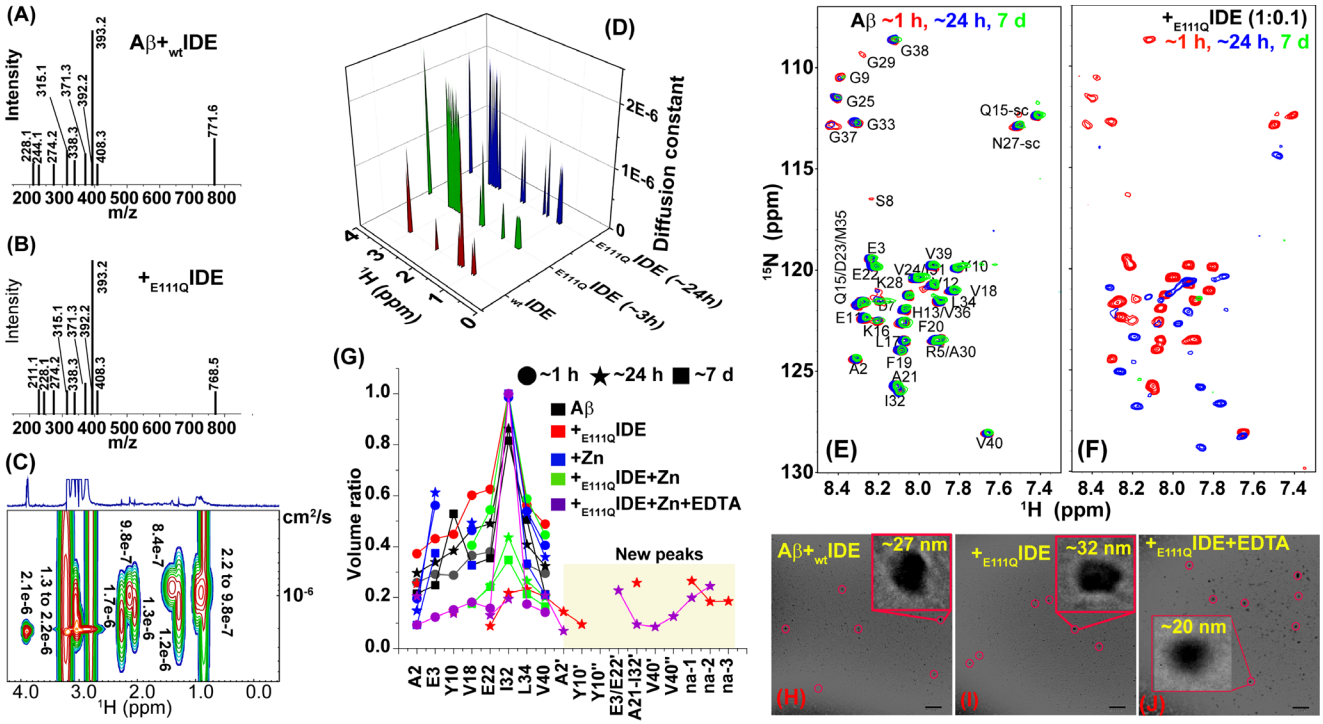


**Figure 1. Characterization of Aβ40 species in the presence of IDE**. (A-B) HPLC-MS spectra revealing the formation of Aβ fragments by $_{wt}$IDE and $_{E111Q}$IDE. 50 μM of Aβ monomers were incubated with 5 μM of IDE for ~12 hours at room temperature prior to HPLC-MS sample preparation. Figs.S4-S6 show the original HPLC-MS spectra. (C) Characterization of $_{E111Q}$IDE cleaved Aβ fragments (see Fig.S8 for $_{wt}$IDE) DOSY). (D) 3D plot showing the diffusion constant (cm$^2$/s) of 25 μM Aβ fragments cleaved by 5 μM $_{E111Q}$IDE. (E-F) 2D $^{15}$N/$^1$H SOFAST-HMQC spectra of 25 μM Aβ40 dissolved in 10 mM sodium phosphate buffer, pH 7.4, 10% $D_2O$ with and without 2.5 μM $_{E111Q}$IDE. (G) Mapping the depletion in residue peak volume and appearance of new peaks as a function of time in Aβ40 in the absence or presence of $_{E111Q}$IDE enzyme, zinc and EDTA. NMR spectra are shown in Figs.1(E, F), 3A, 4B and S13. The peak volume ratio obtained at ~24 h (star) or 7 days (rectangle) is normalized with respect to the corresponding spectrum obtained at ~1 h (circle). New peaks are marked with ' and ", and the unassigned peaks with "na" in (G). (H-J) Negatively stained TEM images of 5 μM Aβ40 in the presence of 0.5 μM $_{wt}$IDE, $_{E111Q}$IDE and $_{E111Q}$IDE+5μM EDTA incubated ~24 hours at room temperature prior to imaging show globular Aβ40 species with size ≥ 20 nm. The scale bar is 200 nm.

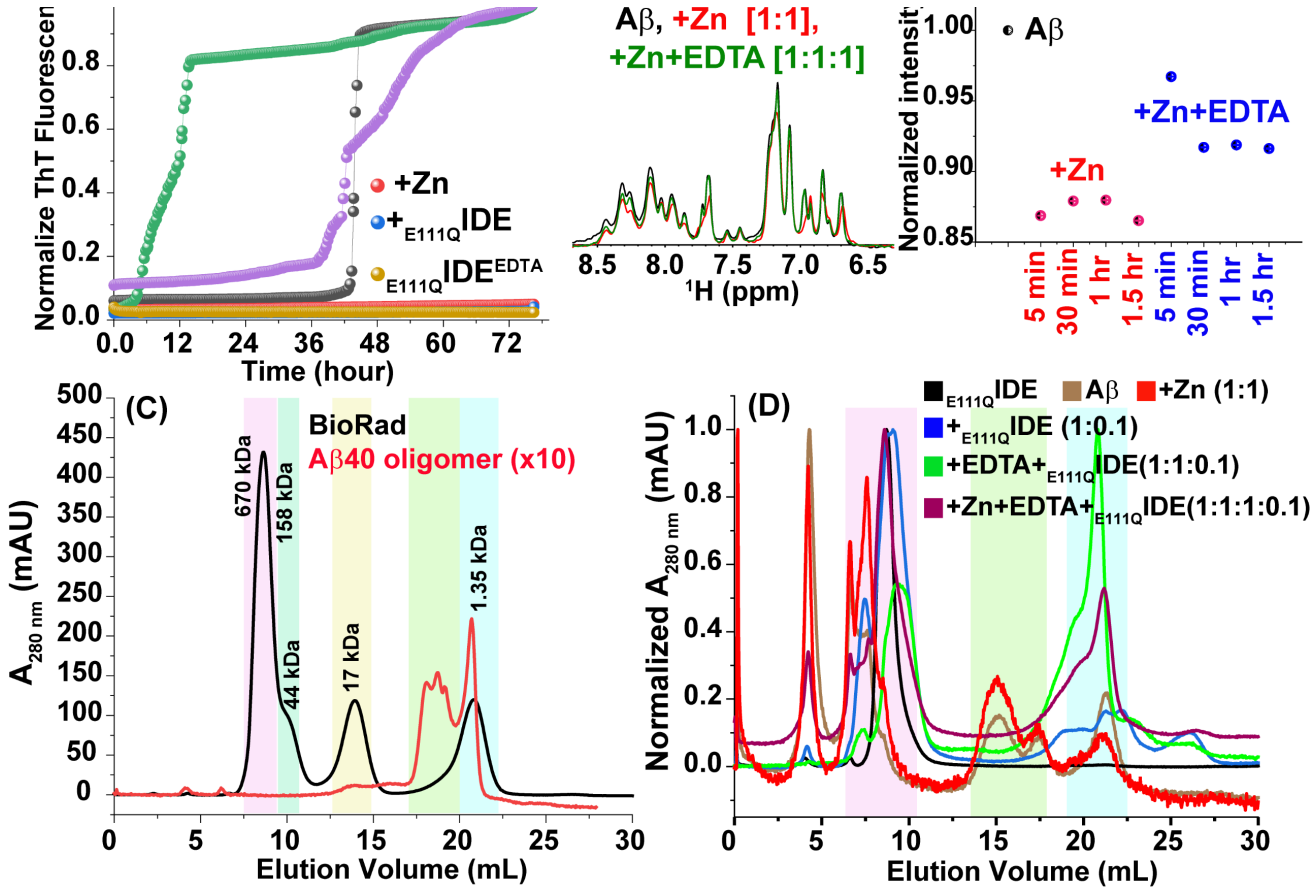


**Figure 2.** Catalytic effect of $_{E111Q}$IDE on Aβ40 in the presence of zinc and EDTA. (A) ThT curve (average from triplicate is shown in Figure S12) representing the aggregation kinetics of 5 μM Aβ40 in the absence or presence of 5 μM zinc, EDTA and 0.5 μM $_{E111Q}$IDE as indicated in colors at 25 °C. (B) $^{1}$H NMR spectra of 25 μM Aβ40 showing a reversible change in signal intensity upon zinc binding and chelation using EDTA at the indicated stoichiometry. The change in signal intensities are normalized with respect to Aβ40 in the absence of any additives. (C-D) Size-profile analysis of 25 μM Aβ40 using SEC. (C) Aβ40 oligomers were prepared in F-12 media (see methods) and characterized in reference to commercially available BioRad protein ladder. (D) SEC of NMR samples used for $^{15}$N/$^{1}$H SOFAST-HMQC (Figs.1, 3 and 4) on day-7. The highlighted colors corresponds to the size distribution indicated in (C).

used NMR to evaluate Aβ40 fragmentation by $_{E111Q}$IDE.

NMR spectra indicate an unstructured conformation incubated for ~1 hour at room temperature, whereas after ~24 hours and 7-days incubations, showed line-broadening indicating a structural rearrangement and aggregation (Fig. 1E). Remarkably, incubation of 1:10 $_{E111Q}$IDE:Aβ40 showed no major changes at ~1 hour, but several new peaks appeared at ~24 hours with substantial line-broadening (Fig. 1F,G). Peak analysis for selected residues showed a ratio of ~10-20% for the new peaks (red stars in Fig. 1G). Strikingly, most of the peaks disappear on day-7 suggesting the $_{E111Q}$IDE-cleaved Aβ40 fragments form large-size aggregates that are not detected by solution NMR (Fig. 1E, green). The size-dependent NMR invisibility can also be correlated to the TEM observations that showed particles of size ~32 nm (Fig. 1I). Next, we monitored the Aβ40 cleavage by $_{E111Q}$IDE at sub-stoichiometric concentration (enzyme:substrate=1:100) to ensure the concentration dependent proteolytic activity as evidenced from ThT fluorescence (Fig. S2). NMR spectra showed Aβ40 fragmentation with the appearance of several new peaks, but a comparatively slow degradation was identified at ~8 hours (Fig. S11). Importantly, unlike the observation at a superstoichiometric concentration of $_{E111Q}$IDE (Fig. 1F), we did not observe severe line-broadening at substoichiometric concentration on day-7. This is most likely due to the difference in the relative kinetics of Aβ40 self-assembly and fragmentation that vary at least in several orders of magnitude. Considering the proteolytic cavity of IDE (volume ~1.3×10$^{4}$ Å$^{3}$) as evidenced from the X-ray structure,[31] the low-ordered NMR visible aggregates that do not fit the active site are not substrates of $_{E111Q}$IDE and are more likely to appear in the $^{15}$N/$^{1}$H spectrum.

Following the NMR observation, that showed size-dependent proteolytic activity of $_{E111Q}$IDE, we next investigated the effect of $_{E111Q}$IDE on the zinc-Aβ40 complex that has been shown to be toxic and prevents degradation by NEP, IDE and matrix metalloprotease.[14,39,40] ThT fluorescence showed retardation and acceleration in Aβ40 aggregation by zinc and EDTA, respectively (Figs. 2A and S12). Notably, while zinc-chelated-IDE abolished Aβ40 fibrillation, zinc-chelated-Aβ40 showed fibrillation in the absence of $_{E111Q}$IDE (but not in the presence) indicating zinc-chelated-Aβ40 is a substrate of $_{E111Q}$IDE. To probe this, $^{1}$H NMR experiments were carried out. A substantial decay in signal intensity

of the Aβ40 fingerprint region (6.5 to 8.5 ppm) was observed when mixed with equimolar zinc indicating the formation of zinc-peptide aggregates (Fig. 2B). Remarkably, zinc chelation by EDTA (1:1) recovered the loss of $^{1}$H signal intensity suggesting dissociation of the Zn-Aβ40 complex to form monomer-like Aβ40 species. This is further verified by size profiling using size-exclusion chromatography (SEC). The Aβ40 oligomers prepared using F-12 media showed an elution profile with a triplet near ~18-19 mL and a singlet near ~21 mL. The SEC peaks are referenced with respect to Bio-Rad's gel filtration standard mixture (Fig. 2C, black) containing thyroglobulin, γ-globulin, ovalbumin, myoglobin, and vitamin B12 (MW 1.35 to 670 kDa). The triplet and singlet observed for Aβ40 oligomers correspond to oligomers and monomers, respectively (Fig. 2C, red). 7-days incubation of Aβ40 monomers showed major populated fibers eluting at the dead volume (~7 mL), small amount of oligomers (~15 mL) and monomers (~21 mL). $_{E111Q}$IDE was observed to elute near ~8 mL, and Zn-Aβ40 complexes depicted monomers, oligomers and larger aggregates (Fig. 2D, black and red). As anticipated, Aβ40 mixed with $_{E111Q}$IDE presented monomers and large aggregates, which agree with TEM observations. Notably, Aβ40 incubated with zinc/EDTA/IDE or EDTA/IDE showed monomers as major population and no oligomer peak (Fig. 2D, green and purple). Taken together, the SEC, ThT fluorescence and NMR results reveal (i) zinc-chelated-$_{E111Q}$IDE is proteolytically degrade Aβ40, and (ii) removal of zinc by EDTA resulted in Zn-Aβ40 complex dissociation and the formation of Aβ40 monomers or low-molecular weight aggregates.

The effect of $_{E111Q}$IDE on the Zn-Aβ40 complex was next monitored using NMR. The 1:1 Zn-Aβ40 complex incubated for ~1 hour showed substantial line-broadening for A2, E3, Y10, E11, V12 and K16 (Fig. S13A), as compared to the Aβ40-alone spectrum (Fig. 1E), in agreement with the reported zinc binding sites.[15,41] Further line-broadening observed for several residues (Fig. 1G, blue squares) on day-7 indicate an increase in the size of Zn-Aβ40 aggregates.[16] Surprisingly, the Zn-Aβ40 complex (25 μM) incubated with 2.5 μM $_{E111Q}$IDE showed no substantial change in the spectrum even after 7 days (Fig. 3A). Unlike the observation for Aβ40 proteolysis by $_{E111Q}$IDE in the absence of zinc, the appearance of new peaks (Fig. 1G, green squares) and the disappearance of existing peaks until day-7 (Fig. 3A) was not observed. These results suggest that zinc bound Aβ40 species are not substrates of $_{E111Q}$IDE due to their large size that cannot be accommodated on IDE's catalytic cavity. No significant changes in signal intensities for Aβ40 mixed with zinc, or zinc and $_{E111Q}$IDE, (Figs. 3B and S13B, 7.5-8.5 ppm) were observed ruling out the possibility of monomer dissociation, proteolysis and fibrillation. Considering the crucial role of zinc in AD pathology,[39] the reported NMR results highlight a dual function for zinc that has been poorly explored.

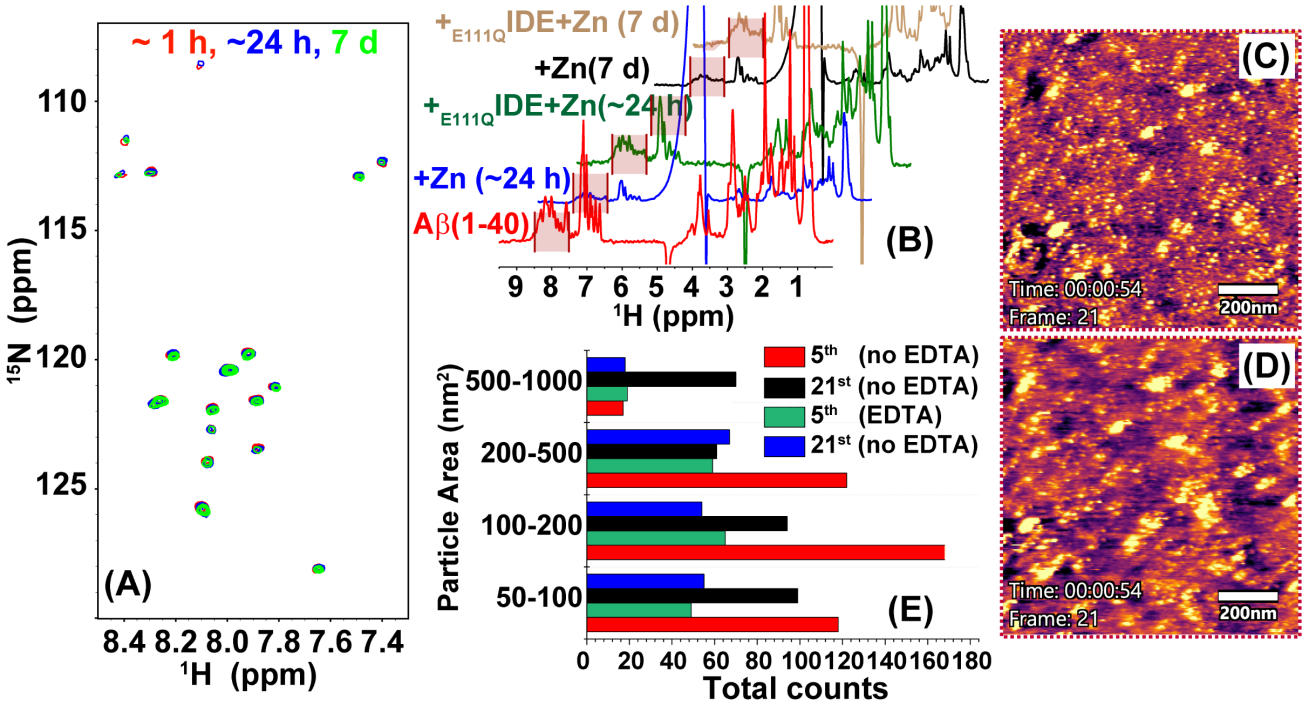


**Figure** 3. Monitoring the proteolytic activity of $_{E111Q}$IDE on Aβ40 in the presence of zinc. (A) Time-lapse NMR spectra of 25 μM Aβ40 co-incubated with 25 μM zinc in the presence of 2.5 μM $_{E111Q}$IDE as indicated in colors. NMR samples were prepared using NaPi buffer, pH=7.4 containing 10% $D_2O$. (B) Decay in $^{1}$H NMR signal of 25 μM Aβ40 co-incubated with 25 μM zinc in the absence or presence of 2.5 μM $_{E111Q}$IDE as a function of time (see Fig.S13B). Real-time monitoring of 5 μM zinc-Aβ (1:1) complex incubated with 0.5 μM $_{E111Q}$IDE in the absence (C) or presence of 5 μM EDTA (D) using HS-AFM. (E) Quantitative analysis of the particle size obtained from the HS-AFM images frame-5 and frame-21 (C-D) using ImageJ. The particles are shown in Figs. S14, S15.

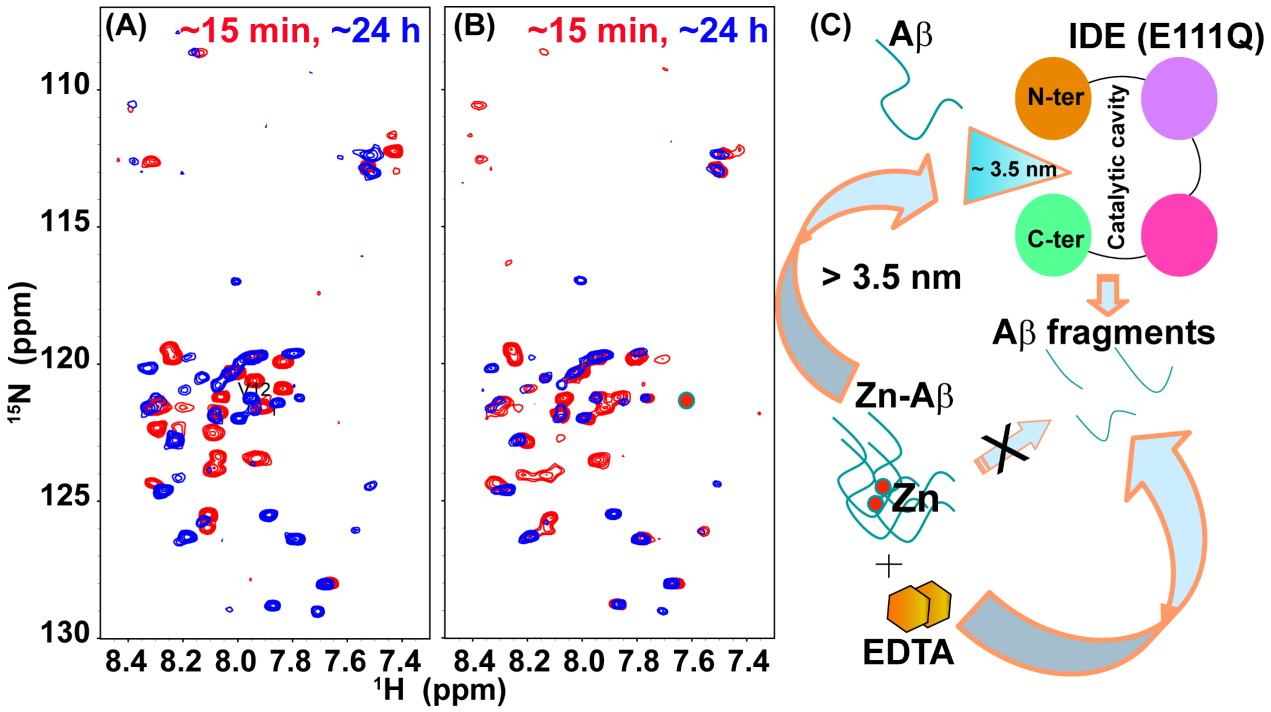


**Figure 4.** Zinc chelation resumes the proteolytic activity of $_{E111Q}$IDE. (A) SOFAST-HMQC spectra of 25 μM $^{15}$N labelled Aβ40 co-incubated with 25 μM EDTA and 2.5 μM $_{E111Q}$IDE. (B) Titration of 25 μM EDTA to pre-incubated 25 μM Aβ40, 25 μM zinc and 2.5 μM $_{E111Q}$IDE. (C) Representation of how zinc impairs IDE's catalytic activity by forming Zn-Aβ complex that does not fit IDE's ≈35 Å active site. Zinc removal from Zn-Aβ complex by EDTA enables the degradation of Aβ by IDE.

Zinc binding enhances the toxic activity of Aβ,[14,39] and as shown here, zinc could also impair IDE's proteolytic activity. To this extent, we next probed the possibility of reversing IDE's activity via zinc removal by chelation with EDTA. HS-AFM was used to probe the efficacy of EDTA to reverse the morphology of Zn-Aβ40 aggregates and generate $_{E111Q}$IDE preferred small aggregates or monomers. Size of zinc-bound-Aβ40 was found to vary from ~5 nm to several hundreds of nm in diameter (Figs. 3C,D and S14). Analysis of particle size (Fig. S14) presented a relatively high number of small particles (area 50-200 nm$^2$); an increase to 500-1000 nm$^2$ was observed highlighting the assembling of small Zn-Aβ40 particles over time (Fig.3E, black bar), whereas EDTA reduced the number of small particles (Fig. S15) as illustrated in Fig. 3E (green bars) and restricted particle fusion and the formation of large aggregates (Figs. 3E and S15). Thus, HS-AFM data revealed the dissociation of small aggregates (area 50-200 nm$^2$) to invisible species, which could be a preferable substrate for IDE.

Time-lapse SOFAST-HMQC experiments were performed to test if the Aβ40 species formed from the Aβ40-Zn complex, due to zinc removal by EDTA-Zn chelation, are substrates of $_{E111Q}$IDE. $_{E111Q}$IDE showed activity when co-incubated with EDTA followed by titration to Aβ40 (Fig. 4A). Appearance of several new peaks at ~24 hours resembled the proteolytic activity of zinc-chelated-$_{E111Q}$IDE (Fig. 4A). Strikingly, when the pre-incubated Zn-Aβ40 aggregates that showed resistance to enzymatic proteolysis (Fig. 3A) titrated with EDTA, several new peaks appeared (Fig. 1G, purple stars) within ~24 hours indicating Aβ40 fragmentation (Fig. 4B). This NMR observation correlates to ThT fluorescence quenching (Fig. 2A, yellow trace) suggesting that zinc-Aβ40 are proteolytically cleaved by $_{E111Q}$IDE in the presence of EDTA.

In conclusion, in this study we have demonstrated the proteolytic activity of an IDE mutant (E111Q) on Aβ40, which has been developed to treat type-2 diabetes, indicating its dual action on type-2 diabetes and AD. Both wild-type and IDE mutant are catalytically active and able to cleave Aβ40 monomers to small fragments. The cleaved Aβ fragments by wild-type IDE or E111Q mutant self-assemble to form morphologically similar globular structures of size ~20-30 nm that are tested to be nontoxic.[30] A key finding in this study is the ability of zinc to generate proteolytic resistant Aβ40 species that are pathologically relevant (Fig. 4C). Zinc binding generates off-pathway Aβ aggregates that grow in size and do not fit to the catalytic cavity (≈35 Å) of IDE (Fig. 4C). Whereas, removal of zinc by EDTA from the Zn-Aβ complex was shown to resume the proteolytic activity of IDE and Aβ fragmentation. This highlights the key role of zinc in AD in

incapacitating the enzymatic degradation of soluble Aβ monomers. Thus, these findings urge the development of potent therapeutic zinc chelating agents to resume the enzymatic degradation of soluble Aβ and prevention of AD progression.

## Experimental Section

Experimental Details are provided in the supporting information.

## Acknowledgements:

This study was supported by NIH (AG048934 to A.R.).

**Keywords:** Aβ • Insulin degrading enzyme • AFM • NMR

## References

[1] G. G. Glenner, C. W. Wong, *Biochem. Biophys. Res. Commun.* **1984**, *120*, 885–890.
[2] C. L. Masters, G. Simms, N. A. Weinman, G. Multhaup, B. L. McDonald, K. Beyreuther, *Proc. Natl. Acad. Sci. U. S. A.* **1985**, *82*, 4245–4249.
[3] Y. J. Chang, Y. R. Chen, *FEBS J.* **2014**, *281*, 2674–2687.
[4] W. D.M., C. C.A., *J. Alzheimer's Dis.* **2008**, *15*, 555–569.
[5] B. R. Sahoo, T. Genjo, T. W. Nakayama, A. K. Stoddard, T. Ando, K. Yasuhara, C. A. Fierke, A. Ramamoorthy, *Chem. Sci.* **2019**, *10*, 3976–3986.
[6] S. Makin, *Nature* **2018**, *559*, S4–S7.
[7] T. J. Esparza, N. C. Wildburger, H. Jiang, M. Gangolli, N. J. Cairns, R. J. Bateman, D. L. Brody, *Sci. Rep.* **2016**, *6*, 1.
[8] T. J. Esparza, H. Zhao, J. R. Cirrito, N. J. Cairns, R. J. Bateman, D. M. Holtzman, D. L. Brody, *Ann. Neurol.* **2013**, *73*, 104–119.
[9] S. A. Kotler, P. Walsh, J. R. Brender, A. Ramamoorthy, *Chem. Soc. Rev.* **2014**, *43*, 6692–6700.
[10] C. J. Maynard, A. I. Bush, C. L. Masters, R. Cappai, Q. X. Li, *Int. J. Exp. Pathol.* **2005**, *86*, 147–159.
[11] B. R. Sahoo, M. E. Bekier, Z. Liu, V. Kocman, A. K. Stoddard, G. M. Anantharamaiah, J. Nowick, C. A. Fierke, Y. Wang, A. Ramamoorthy, *J. Mol. Biol.* **2020**, *432*, 1020.
[12] I. Peters, U. Igbavboa, T. Schütt, S. Haidari, U. Hartig, X. Rosello, S. Böttner, E. Copanaki, T. Deller, D. Kögel, et al., *Biochim. Biophys. Acta - Biomembr.* **2009**, *1788*, 964–972.
[13] G. P. Eckert, W. G. Wood, W. E. Müller, *Subcell. Biochem.* **2005**, *38*, 319–337.
[14] M. C. Lee, W. C. Yu, Y. H. Shih, C. Y. Chen, Z. H. Guo, S. J. Huang, J. C. C. Chan, Y. R. Chen, *Sci. Rep.* **2018**, *8*, 1.
[15] N. Rezaei-Ghaleh, K. Giller, S. Becker, M. Zweckstetter, *Biophys. J.* **2011**, *101*, 1202–1211.
[16] D. Noy, I. Solomonov, O. Sinkevich, T. Arad, K. Kjaer, I. Sagi, *J. Am. Chem. Soc.* **2008**, *130*, 1376–1383.
[17] V. Tõugu, A. Tiiman, P. Palumaa, *Metallomics* **2011**, *3*, 250.
[18] S. Bolognin, L. Messori, D. Drago, C. Gabbiani, L. Cendron, P. Zatta, *Int. J. Biochem. Cell Biol.* **2011**, *43*, 877–885.
[19] F. Bellia, G. Grasso, *J. Mass Spectrom.* **2014**, *49*, 274–279.
[20] G. Grasso, F. Salomone, G. R. Tundo, G. Pappalardo, C. Ciaccio, G. Spoto, A. Pietropaolo, M. Coletta, E. Rizzarelli, in *J. Inorg. Biochem.*, **2012**, pp. 351–358.
[21] G. Grasso, A. Pietropaolo, G. Spoto, G. Pappalardo, G. R. Tundo, C. Ciaccio, M. Coletta, E. Rizzarelli, *Chem. - A Eur. J.* **2011**, *17*, 2752–2762.
[22] Z. Zhao, Z. Xiang, V. Haroutunian, J. D. Buxbaum, B. Stetka, G. M. Pasinetti, *Neurobiol. Aging* **2007**, *28*, 824.
[23] S. M. Huang, A. Mouri, H. Kokubo, R. Nakajima, T. Suemoto, M. Higuchi, M. Staufenbiel, Y. Noda, H. Yamaguchi, T. Nabeshima, et al., *J. Biol. Chem.* **2006**, *281*, 17941–17951.
[24] E. A. Eckman, D. K. Reed, C. B. Eckman, *J. Biol. Chem.* **2001**, *276*, 24540–24548.
[25] A. E. Roher, T. C. Kasunic, A. S. Woods, R. J. Cotter, M. J. Ball, R. Fridman, *Biochem. Biophys. Res. Commun.* **1994**, *205*, 1755–1761.
[26] R. J. Baranello, K. L. Bharani, V. Padmaraju, N. Chopra, D. K. Lahiri, N. H. Greig, M. A. Pappolla, K. Sambamurti, *Curr. Alzheimer Res.* **2015**, *12*, 32–46.
[27] E. Malito, R. E. Hulse, W. J. Tang, *Cell. Mol. Life Sci.* **2008**, *65*, 2574–2585.
[28] M. C. Liao, W. E. Van Nostrand, *Biochemistry* **2010**, *49*, 1127–1136.
[29] A. Bulloj, M. C. Leal, E. I. Surace, X. Zhang, H. Xu, M. D. Ledesma, E. M. Castaño, L. Morelli, *Mol. Neurodegener.* **2008**, *3*, 22.
[30] E. Hubin, F. Cioffi, J. Rozenski, N. A. J. Van Nuland, K. Broersen, *Biochim. Biophys. Acta - Gen. Subj.* **2016**, *1860*, 1281–1290.
[31] Y. Shen, A. Joachimiak, M. Rich Rosner, W. J. Tang, *Nature* **2006**, *443*, 870–874.

[32] R. Deprez-Poulain, N. Hennuyer, D. Bosc, W. G. Liang, E. Enée, X. Marechal, J. Charton, J. Totobenazara, G. Berte, J. Jahklal, et al., *Nat. Commun.* **2015**, *6*, 8250.
[33] R. K. Perlman, B. D. Gehm, W. L. Kuo, M. R. Rosner, *J. Biol. Chem.* **1993**, *268*, 21538–21544.
[34] B. C. Miller, E. A. Eckman, K. Sambamurti, N. Dobbs, K. Martin Chow, C. B. Eckman, L. B. Hersh, D. L. Thiele, *Proc. Natl. Acad. Sci. U. S. A.* **2003**, *100*, 6221–6226.
[35] H. Im, M. Manolopoulou, E. Malito, Y. Shen, J. Zhao, M. Neant-Fery, C. Y. Sun, S. C. Meredith, S. S. Sisodia, M. A. Leissring, et al., *J. Biol. Chem.* **2007**, *282*, 25453–25463.
[36] M. B. de Tullio, V. Castelletto, I. W. Hamley, P. V. Martino Adami, L. Morelli, E. M. Castaño, *PLoS One* **2013**, *8*, e59113.
[37] L. Morelli, R. E. Llovera, I. Mathov, L. F. Lue, B. Frangione, J. Ghiso, E. M. Castaño, *J. Biol. Chem.* **2004**, *279*, 56004.
[38] S. K. Sharma, E. Chorell, P. Steneberg, E. Lindahl, H. Edlund, P. Wittung-Stafshede, *Sci. Rep.* **2015**, *5*, 1–10.
[39] N. Watt, I. Whitehouse, N. Hooper, *Int. J. Alzheimer's Dis.* **2010**, *2011*.
[40] P. J. Crouch, D. J. Tew, T. Du, D. N. Nguyen, A. Caragounis, G. Filiz, R. E. Blake, I. A. Trounce, C. P. W. Soon, K. Laughton, et al., *J. Neurochem.* **2009**, *108*, 1198–1207.
[41] B. Alies, A. Conte-Daban, S. Sayen, F. Collin, I. Kieffer, E. Guillon, P.Faller, C.Hureau, *Inorg. Chem.* **2016**, *55*, 10499.

# Graphical abstract